Spin-Flip Scattering Cross Section for Conduction Electrons of Foreign Atoms in Lithium and Sodium. I*†

J. R. ASIK,‡ M. A. BALL,§ AND C. P. SLICHTER
Department of Physics and Materials Research Laboratory, University of Illinois, Urbana, Illinois 61801
(Received 9 December 1968)

We have measured the spin-flip scattering cross section for conduction electrons of impurities in metallic sodium and impurities in metallic lithium. The cross sections are deduced from the measurements of the dependence on impurity concentration of the linewidth of the conduction-electron spin resonance. Since the apparatus was an X-band superheterodyne spectrometer and the samples were small particles of about 10-μ diam, the Dyson theory must be applied to relate measured linewidth to relaxation time and thus to cross section. A simple theoretical analysis is applied which involves the numerical solution of the non-spin-flip scattering by a screened Coulomb potential whose screening length is adjusted so that the s, p, and d scattering phase shifts satisfy the Friedel sum rule. We then orthogonalize these solutions to the core states of the impurity atom. Using these orthogonalized wave functions and assuming the spin-flip scattering results from a coupling of the electron spin to its orbital motion in the vicinity of the nucleus of the impurity, we use perturbation theory to compute a spin-flip scattering cross sections which has no adjustable parameters. The result accounts well for the magnitudes and trends as one moves down and across the periodic table for those impurities whose valence differs from that of the host by 0, 1, or 2 units. The theory does *not* account for the existence or position of a maximum as one moves across the periodic table.

I. INTRODUCTION

THIS paper has two major purposes.[1] The first is to present data on the spin-flip scattering cross section for conduction electrons colliding with nonmagnetic impurities in metallic lithium and sodium. The cross sections are deduced from the experimental study of conduction-electron spin-resonance (CESR) relaxation time T_1 in dilute alloys. The second purpose is to present a simple orthogonalized-plane-wave (OPW) theory of this relaxation time. In a second paper we present a more extensive theory which accounts in part for some of those aspects not included in the OPW theory but which still leaves important discrepancies between theory and experiment.

The first paramagnetic resonance absorption in metals due to conduction electrons was observed in sodium in 1952 by Griswold, Kip, and Kittel.[2] Feher and Kip[3] later (in 1954) made a systematic search for CESR in various metals and found resonances in Li, K, Be, as well as Na. More recently CESR has been observed in Cs,[4] Rb,[5,6] Cu,[7] Al,[8] and Ag.[9] The pioneering work of Feher and Kip showed that there are at least two contributions to the T_1 of the conduction electrons:

$$1/T_1=(1/T_1)_{\text{phonons}}+(1/T_1)_{\text{impurities}}. \quad (1)$$

The temperature dependence (phonon contribution) of the CESR spin-lattice relaxation time is due to the modulation of the spin-orbit interaction by thermal-lattice vibrations. In this paper we are concerned only with the impurity contribution to T_1.

One determines the spin-lattice relaxation time indirectly by using the equality between T_1 and T_2, the transverse relaxation time. A line-shape analysis gives the relationship between the linewidth ΔH, which can be directly measured, and T_2. Yafet[10] has recently discussed the question of the equality of T_1 and T_2. His conclusion is that T_1 and T_2 are equal in isotropic (cubic) crystals but may be different in anisotropic crystals. Physically, one expects that the high relative speed of the conduction electrons and the screening of the electron-electron interaction should drastically reduce the broadening effect of the spin-spin interactions. This effect is analogous to the motional narrowing[11] of NMR lines.

In this paper we analyze a new type of experiment: measurement of the effect of impurities on the spin-orientation lifetime of conduction electrons.[12] The

* Research supported in part by the U. S. Atomic Energy Commission, under Contract No. AT(11-1)-1198.

† Based on a thesis submitted by J. R. Asik in partial fulfillment of the requirements for the Ph.D. degree in physics, in the Graduate College of the University of Illinois, 1966.

‡ Present address: IBM Watson Research Center, Yorktown Heights, N. Y. 10598.

§ Present address: Department of Applied Mathematics, The University, Liverpool, England.

[1] Two preliminary accounts have already appeared: J. R. Asik, M. A. Ball, and C. P. Slichter, Phys. Rev. Letters **16**, 740 (1966); in Proceedings of the Fourteenth Colloque Ampère, 1967, p. 389 (unpublished).

[2] T. W. Griswold, A. F. Kip, and C. Kittel, Phys. Rev. **88**, 951(L) (1952).

[3] G. Feher and A. F. Kip, Phys. Rev. **98**, 337 (1955).

[4] R. A. Levy, Phys. Rev. **102**, 31 (1956).

[5] S. Schultz and M. R. Shanabarger, Phys. Rev. Letters **16**, 178 (1966).

[6] W. M. Walsh, Jr., L. W. Rupp, Jr., and P. H. Schmidt, Phys. Rev. Letters **16**, 181 (1966).

[7] S. Schultz and C. Latham, Phys. Rev. Letters **15**, 148 (1965).

[8] S. Schultz, G. Dunifer, and C. Latham, Phys. Letters **23**, 192 (1966).

[9] S. Schultz and M. R. Shanabarger, Phys. Rev. Letters **19**, 749 (1967).

[10] Y. Yafet, in *Solid State Physics*, edited by F. Seitz and D. Turnbull (Academic Press Inc., New York, 1963), Vol. 14.

[11] For example, see C. P. Slichter, *Principles of Magnetic Resonance* (Harper & Row Publishers, Inc., New York, 1963), p. 153.

[12] Previous published measurements are *Na*Hg: N. S. Garif'ianov and M. A. Starikov, Zh. Eksperim. i Teor. Fiz. **35**, 798 (1958) [English transl.: Soviet Phys.—JETP **8**, 553 (1959)]; *Li*Mg: G. D. Wignall, J. E. Enderby, C. E. W. Hahn, and J. M. Titman, Phil. Mag. **12**, 433 (1965); *Li*Mg, *Li*Zn, and *Li*Ag: C. E. W. Hahn and J. E. Enderby, Proc. Phys. Soc. (London) **92**, 418 (1967).

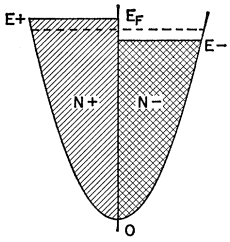

FIG. 1. Hypothetical spin polarization in the absence of an applied magnetic field. The number density of spin-up (-down) electrons is N_+ (N_-) and the Fermi level is E_+ (E_-). The equilibrium Fermi level is E_F.

spin-flip scattering cross sections for Fermi electrons of 14 impurities in lithium metal and 7 impurities in sodium metal have been measured directly. The existence of a nonvanishing spin-flip cross section implies that there is an impurity contribution to the spin-lattice relaxation rate. This contribution can be determined by measuring the effect of various concentrations of added impurity on the linewidth of the CESR.[13] In several cases we have observed solubility limits for very dilute ($<10^{-2}$ at.%) alloys. In other cases, no effect was observed, which we attribute to the impossibility of even dilute solubility. The large spin-orbit interaction characteristic of the high-Z elements, such as Au and Tl, enables them to produce easily measurable effects for fractional concentrations as low as 1 atom in 10^7.

For monovalent impurities, such as Ag and Au, the experimental results are well accounted for by an OPW theory which considers the interaction of the conduction-electron spin with its orbital motion in the electric field of the impurity atom (spin-orbit coupling) as a perturbation. For nonmonovalent impurities, we represent the electrostatic effect of the impurity by a screened Coulomb potential and again take the spin-orbit interaction as a perturbation. The theory accounts for our experimental results for impurities having valence differences of ± 1 with respect to Li or Na. For the high-Z elements of groups IIIA and IVA, our simple theory deviates from the results. These deviations are especially large for the group-IVA impurities Sn and Pb.

The physical idea behind impurity-induced spin-flip scattering of conduction electrons can be described in the following crude manner. In metals such as Li or Na in which the spin-orbit interaction with the host atoms is small, the conduction electrons are described by Bloch functions in which the spin state is quantized predominantly up or down. Suppose that a single impurity with strong spin-orbit interaction is introduced substitutionally into the lattice. In being scattered by the impurity, an electron of given spin acquires a certain admixture of the opposite spin state, since the spin and orbit are coupled while the electron is near the impurity. This coupling therefore has induced transitions between spin-up and spin-down Bloch states. The transition rate is much larger than one would calculate using plane waves or host-lattice Bloch functions in the scattering problem, since the wave function near the impurity more closely resembles a mixture of the impurity-free-atom wave functions than plane waves or host-atom atomic functions.

In Sec. II, we present the perturbation theory for impurity-induced spin-lattice relaxation. The experimental apparatus and procedure are discussed in Sec. III. The experimental results are given and compared with theory in Sec. IV, which, in addition, contains a discussion of possible explanations for the observed nonmonotonic variation of the spin-flip cross sections.

II. THEORY

A. Spin-Lattice Relaxation

We will take the band structure of the host metal to be described by spherical energy surfaces. To calculate T_1, it is convenient to assume that *initially* the number of electrons per unit volume with spin up N_+ and the number density of electrons with spin down N_- differ from their thermal-equilibrium values, but that the kinetic energies of each spin distribution are in thermal equilibrium with the lattice. This latter condition results from frequent electron-phonon collisions. For simplicity we assume the static field to be zero, so that in thermal equilibrium $N_+=N_-$. We suppose that by some means the populations are made to be unequal initially. (Conceptually this could be achieved by applying a static field for a time long compared to T_1, and then suddenly switching it off. In practice this would be difficult because of the shortness of T_1.) Thus, since the Zeeman energy of the spins is zero, the bottoms of the two spin distributions coincide, but the tops do not. There are thus two Fermi energies: E_+ and E_-. The equilibrium Fermi energy is E_F (see Fig. 1). Let the density of states in energy be $\rho'(E)$ for each spin distribution.

The excess spin population is therefore given by

$$N_+-N_-=\int [f_+(E)-f_-(E)]\rho'(E)dE \qquad (2)$$

$$=\int \frac{\partial f}{\partial E_F}\Delta E\rho'(E)dE, \qquad (3)$$

where $\Delta E=E_+-E_-$, and f_+ is the Fermi function for spin-up electrons. To obtain (3) from (2), we assume that the population difference N_+-N_- is small compared to the total electron density $N_0=N_++N_-$. Using the relation $\partial f/\partial E_F=\delta(E-E_F)$, where $\delta(x)$ is

[13] Recently a powerful indirect technique has been developed to measure this contribution. This technique involves measuring the temperature dependence of the T_1 of dilute paramagnetic ions dissolved in metals containing small additions of a second impurity, which can be transition-metal or nontransition-metal impurities. The effect of the second impurity is to open up the bottleneck to conduction-electron-spin relaxation. See A. C. Gossard, A. J. Heeger, and J. H. Wernick, J. Appl. Phys. **38**, 1251 (1967); also, A. C. Gossard, T. Y. Kometani, and J. H. Wernick, *ibid.* **39**, 849 (1968); Y. Yafet, *ibid.* **39**, 853 (1968).

the Dirac δ function, Eq. (3) becomes

$$N_+-N_-=\Delta E\rho'(E_F). \tag{4}$$

The rate equation defining T_1 is

$$d(N_+-N_-)/dt=-(N_+-N_-)/T_1. \tag{5}$$

The total rate of change of N_+ can be broken down into two contributions:

$$\frac{dN_+}{dt}=\frac{dN_+}{dt}\bigg|_{-\to+}-\frac{dN_+}{dt}\bigg|_{+\to-}. \tag{6}$$

Let us introduce a microscopic transition probability $W(\mathbf{k}+,\mathbf{k}'-)$ to describe the scattering from a state $|\mathbf{k}+)$ to a state $|\mathbf{k}'-)$. The second term on the right side of (6) can be written

$$\frac{dN_+}{dt}\bigg|_{+\to-}=\int W(\mathbf{k}+,\mathbf{k}'-)f_+(\mathbf{k})[1-f_-(\mathbf{k}')] \times\rho'(E)\rho'(E')dEdE'\frac{d\Omega d\Omega'}{(4\pi)^2}. \tag{7}$$

In (7) we use E for $E_\mathbf{k}$, etc. Making use of the fact that $f_+(\mathbf{k})-f_-(\mathbf{k})=(\Delta E)\partial f/\partial E_F=(\Delta E)\delta(E-E_F)$, the expression for the rate of change of N_+ becomes

$$\frac{dN_+}{dt}=-\Delta E\int W(\mathbf{k}+,\mathbf{k}'-)\delta(E-E_F) \times\rho'(E)\rho'(E')dEdE'\frac{d\Omega d\Omega'}{(4\pi)^2}. \tag{8}$$

We now introduce a spin-dependent scattering potential V which is produced by substitutional impurities. Using Fermi's "golden rule" of perturbation theory,

$$W(\mathbf{k}+,\mathbf{k}'-)=\frac{2\pi}{\hbar}|(\mathbf{k}+|V|\mathbf{k}'-)|^2\delta(E-E'). \tag{9}$$

Substituting this into Eq. (8) and making use of the two δ functions, one finds

$$\frac{dN_+}{dt}=-\Delta E\frac{2\pi}{\hbar}\rho'^2(E_F)\int|(\mathbf{k}_F+|V|\mathbf{k}_F'-)|^2\frac{d\Omega d\Omega'}{(4\pi)^2}. \tag{10}$$

Defining

$$\langle V^2\rangle_F=\int|(\mathbf{k}_F+|V|\mathbf{k}_F'-)|^2\frac{d\Omega d\Omega'}{(4\pi)^2}, \tag{11}$$

and using Eqs. (4), (5), (10), and (11), we arrive at an expression for T_1:

$$1/T_1=(2\pi/\hbar)\langle V^2\rangle_F\rho(E_F). \tag{12}$$

In Eq. (12) we have introduced $\rho(E_F)$, the density of states including both spin orientations, which equals $2\rho'(E_F)$.

If the perturbing potential V is produced by a concentration c of impurity atoms, we can write

$$V=\sum_{i=1}^{N_0c}V_i, \tag{13}$$

where V_i is the potential due to the ith impurity atom and N_0 the number of host atoms per unit volume. The usual approximation in the case of dilute alloys is to assume incoherent scattering. We thus obtain

$$1/T_1=(2\pi/\hbar)N_0c\langle V_1^2\rangle_F\rho(E_F), \tag{14}$$

where V_1 is the spin-dependent perturbing potential of a single-impurity atom. Equation (14) predicts that the spin-lattice relaxation rate varies linearly with the concentration of impurities.

B. Spin-Orbit Interaction

We take as the perturbation V_1 the spin-orbit interaction[14] of a conduction electron in the electric field of a single-impurity atom, i.e.,

$$V_1=(e\hbar/2m^2c^2)\mathbf{s}\cdot(\mathbf{E}\times\mathbf{p})=\lambda(r)\mathbf{s}\cdot\mathbf{l}, \tag{15}$$

where e is the magnitude of the electronic charge, $\mathbf{E}$ is the electric field due to the impurity, and $\mathbf{s}$ and $\mathbf{l}$ are dimensionless operators. Since $\mathbf{E}$ is large only in the atomic core, it is proper to take $\mathbf{E}$ to be radial and derived from a central potential A_0:

$$\mathbf{E}=-\frac{\mathbf{r}}{r}\frac{dA_0}{dr}. \tag{16}$$

Thus, the coupling function $\lambda(r)$ is given by

$$\lambda(r)=-\frac{e\hbar^2}{2m^2c^2}\frac{1}{r}\frac{dA_0}{dr}. \tag{17}$$

Let us consider the quantity

$$\langle V_1^2\rangle_F=\int|(\mathbf{k}_F+|V|\mathbf{k}_F'-)|^2\frac{d\Omega d\Omega'}{(4\pi)^2} \tag{18}$$

$$=\sum_{p,p'=x,y}(+|s_p|-)(-|s_{p'}|+) \times\int(\mathbf{k}_F|\lambda l_p|\mathbf{k}_F')(\mathbf{k}_F'|\lambda l_{p'}|\mathbf{k}_F)\frac{d\Omega d\Omega'}{(4\pi)^2}. \tag{19}$$

We can symmetrize the orbital and spin parts of Eq. (19) and thus obtain the result

$$\langle V_1^2\rangle_F=\tfrac{1}{4}\sum_{p,p'=x,y}(+|s_ps_{p'}+s_{p'}s_p|+) \times\int[(\mathbf{k}_F|\lambda l_p|\mathbf{k}_F')(\mathbf{k}_F'|\lambda l_{p'}|\mathbf{k}_F) +(\mathbf{k}_F|\lambda l_{p'}|\mathbf{k}_F')(\mathbf{k}_F'|\lambda l_p|\mathbf{k}_F)]\frac{d\Omega d\Omega'}{(4\pi)^2}. \tag{20}$$

[14] R. J. Elliott, Phys. Rev. **96**, 266 (1954).

Since

$$s_p s_{p'} + s_{p'} s_p = 0, \quad \text{if} \quad p \neq p' \tag{21}$$

and since the integrals involving l_x and l_y are symmetric, Eq. (20) reduces to

$$\langle V_1^2 \rangle_F = \frac{1}{2} \int |(\mathbf{k}_F|\lambda(r) l_x|\mathbf{k}_F')|^2 \frac{d\Omega d\Omega'}{(4\pi)^2}. \tag{22}$$

C. OPW Perturbation Theory for Monovalent Impurities

In order to evaluate Eq. (22), we need to know the orbital wave functions $|\mathbf{k}_F)$. Let us first consider monovalent substituents, i.e., those that have the same valence as Li or Na. This case is the simplest because no complications from screening of excess ionic charge arise. The states $|\mathbf{k}_F)$ are the exact one-electron states of electrons moving in the electric field of the lattice and the impurity, but neglecting the spin-orbit interaction V_1. However, it is not correct to take the states $|\mathbf{k}_F)$ to be the Bloch states of the pure metal, since the potential in the vicinity of the impurity atom is different from that of Li or Na despite the identity of valence.

The simplest approximation for impurity atoms which produce large scattering compared to their hosts is to take the $|\mathbf{k})$'s as plane-wave states orthogonalized to the impurity core states. Orthogonalization guarantees that the Pauli exclusion principle is satisfied and produces atomiclike oscillations in the wave function in the vicinity of the nucleus.[15] Thus, we write

$$|\mathbf{k}_F) = e^{i\mathbf{k}_F \cdot \mathbf{r}} - \sum_q a_q |q), \tag{23}$$

where

$$a_q = (q|e^{i\mathbf{k}_F \cdot \mathbf{r}}). \tag{24}$$

The states $|q)$ are the core functions of the impurity atom, and the plane wave is normalized to a volume of 1 cm^3. We assume that the concentration of impurities is small and therefore neglect the change in normalization due to orthogonalization.

Let us now specialize to atomic s and p functions. If $|q)$ is an s state, the contribution to the spin-orbit matrix element is zero. The three p orbital states can be written

$$|q) = xf(r), yf(r), zf(r). \tag{25}$$

The overlap integral a_{np} for the np atomic state is defined as

$$(n,xf(r)|e^{ikFx}) = a_{np}. \tag{26}$$

We label the coordinate axes of $\mathbf{k}$ as X, Y, and Z. If $\mathbf{k}$ is parallel to Z, then

$$|q) = \sum_{q'=Xf(r),Yf(r),Zf(r)} c_{q,q'} |q'). \tag{27}$$

Thus, we have

$$a_q = (q|e^{i\mathbf{k}_F \cdot \mathbf{r}}) = a_{np} c_{qZ}, \tag{28}$$

where we have written Z for $Zf(r)$. In this notation, the spin-orbit matrix element becomes

$$(\mathbf{k}_F'|\lambda(r) l_x|\mathbf{k}_F) = \sum_{q,q'} a_{np}^2 c_{q'Z} c_{qZ} (q'|\lambda(r) l_x|q). \tag{29}$$

Making use of the fact that $c_{qZ} = \cos(q,Z)$, it can be shown without difficulty that

$$\langle V_1^2 \rangle_{Fnp} = (1/18) a_{np}^4 \sum_{q,q'} |(q'|\lambda(r) l_x|q)|^2. \tag{30}$$

If we take λ_{np} to be the spin-orbit coupling constant of the core state np, then

$$\lambda_{np} = |(n,zf(r)|\lambda(r) l_x|n,yf(r))|. \tag{31}$$

In Eq. (30), the only nonvanishing matrix elements are those for which $q = yf(r)$, $q' = zf(r)$ and $q = zf(r)$, $q' = yf(r)$. Then the final expression for the p-state contribution is

$$\langle V_1^2 \rangle_{Fnp} = \tfrac{1}{9} a_{np}^4 \lambda_{np}^2. \tag{32}$$

In the Appendix we show that the contribution from a set of d-core orbitals to $\langle V_1^2 \rangle_F$ is

$$\langle V_1^2 \rangle_{Fnd} = \tfrac{1}{5} a_{nd}^4 \lambda_{nd}^2. \tag{33}$$

In the Appendix it is also shown that the most general expression for $\langle V_1^2 \rangle_F$ is

$$\langle V_1^2 \rangle_F = \sum_{n,n',l} \frac{l(l+1)}{6(2l+1)} a_{n'l}^2 a_{nl}^2 \lambda_{nl,n'l}^2, \tag{34}$$

where

$$\lambda_{nl,n'l} = |(nl|\lambda(r)|n'l)|. \tag{35}$$

Equation (34) contains two types of contributions. The direct contribution is given by the $n' = n$ terms, while the indirect (or core-core) contribution arises from the $n' \neq n$ terms.

D. Perturbation Theory for Nonmonovalent Impurities

When the valence of the impurity differs from the host, the excess or deficiency of ionic charge must be screened. Since a single impurity adds a negligible total number of electrons to the band, the screening results from a change in the amplitude of the wave function of band electrons at the impurity, and not from a change in the number of occupied states. Thus, if the impurity has two valence electrons, there must be approximately a charge of two electrons in the impurity atomic cell. This implies that a typical band wave function is $\sqrt{2}$ bigger within the impurity cell. Using Eqs. (14) and (32), this leads to an increase in linewidth by approximately $(\sqrt{2})^4 = 4$. Roughly, we expect nontransition-metal impurities in a given periodic row to produce a V^2 dependence for ΔH, where V is the number of valence electrons of the impurity.

[15] J. M. Ziman, *Principles of the Theory of Solids* (Cambridge University Press, Cambridge, England, 1964), p. 93.

In this paper we represent the impurity potential $V_1(r)$ by a screened Coulomb potential,[16]

$$V_1(r) = -(Z_v e^2/r)e^{-\alpha r}. \quad (36)$$

In Eq. (36), Z_v is the valence difference between the impurity atom and the host. The screening parameter α in each case is adjusted so that the s, p, d, $\cdots$, phase shifts η_0, η_1, η_2, $\cdots$, satisfy the Friedel sum rule,[17]

$$Z_v = -\frac{2}{\pi}\sum_{l=0}^{\infty}(2l+1)\eta_l. \quad (37)$$

The radial equation satisfied by the lth radial wave function $\phi_l(r)$, is

$$\frac{d^2\phi_l}{dr^2} + k_F^2\phi_l + \frac{2Z_v}{a_0 r}e^{-\alpha r}\phi_l - \frac{l(l+1)}{r^2}\phi_l = 0, \quad (38)$$

assuming that the effective mass is 1. In Eq. (38), a_0 is the Bohr radius. If $Z_v=0$, the solution to Eq. (38) is the familiar result $rj_l(k_F r)$, where j_l is the spherical Bessel function. At large distances, $r \gg 1/\alpha$, $\phi_l(r)$ has sinusoidal variation. For $Z_v \neq 0$, Eq. (38) must be solved numerically. For the potential given by Eq. (36), we refer to ϕ_l as a screened Coulomb function.

III. EXPERIMENTAL TECHNIQUE

A. Apparatus

The CESR linewidth measurements were made on a fairly conventional single-klystron superheterodyne EPR spectrometer operating at X band. An afc system was employed to frequency-lock the klystron to the sample cavity. The magnet is a Harvey-Wells 12-in. electromagnet homogeneous to 0.1 G across the sample and stable to 1 part in 10^5. Magnetic field modulation at 35 Hz and lock-in detection were also used. At all times the peak-to-peak modulation amplitude was kept less than $\frac{1}{5}$ of the CESR linewidth, and the time necessary to pass through the line was kept greater than 15 time constants of the lock-in amplifier. The first derivative line shape together with proton-frequency magnetic field markers were recorded on a strip chart recorder.

Most of the measurements were made at 300°K, although a few were made at 77°K and also when the alloys were in the liquid state. The ESR samples consisted of small (approximately 20 μ) metallic particles dispersed in paraffin and contained in 4-mm-diam Pyrex tubing about 1 cm long. The ends of the tubes were sealed from the atmosphere with pure paraffin. The metallic filling factor was about 50%. The samples were held in the center of a full wave TE_{102} cavity with styrofoam. The long dimension of the sample was positioned parallel to the microwave H_1.

With the sample sizes used, sample cavity Q's of 1000 to 1500 were obtained. The sensitivity of the spectrometer enabled resonance lines, 250 G wide for lithium alloys and 125 G wide for sodium alloys, to be accurately measured.

B. Samples

The ESR samples were prepared in two steps. The first involved the preparation of the alkali-metal alloy, and the second involved the dispersing of the metal. All operations involving lithium or sodium were carried out either in a recirculating drying box filled with high-purity argon or under oil, and while the metal surface was coated with well-degassed mineral oil.

The alloys were prepared using 99.983% lithium metal[18] and 99.9% sodium metal.[19] When dispersed, the lithium showed a temperature-independent linewidth of less than 1 G, whereas the sodium showed 6 G at 300°K and 2 G at 77°K.

The mechanical preparation of the alloys was performed in the argon-filled dry box. This preparation involved scrape cleaning the surface of previously degreased alkali metal, weighing it, and embedding a known amount of impurity metal well into the body of the alkali. The alloying, except for some highly concentrated lithium-magnesium alloys, was done in degassed mineral oil in a sealed stainless-steel beaker. The alloying was done outside the dry box on an electric hot plate. Alloying proceeded for at least 2 h in all cases. After cooling, the alloy chunk was cut into small pieces and examined by eye for homogeneity. For very dilute alloys, the sample alloys were made using the first alloy as a master alloy. At least two independent master alloys were always prepared.

For the more concentrated lithium-magnesium alloys, the alloying was done in a tantalum crucible. The crucible sat at the bottom of a tantalum furnace tube containing pure argon. The tube was heated to 700°C by an electric furnace. An undoped lithium sample treated this way showed no additional line broadening. In the region of overlap with mineral-oil alloying, there was excellent agreement in measured linewidths (see Fig. 9).

The purities of the doping metals were 99.95% or better in all cases, except for Hg, which was 99.9% pure. Good agreement was found among magnesium-doped alloys in which 99.95 or 99.995% Mg was used (see Fig. 9). The purity of the aluminum was 99.999%.

The alkali-metal and alkali-alloy dispersions were made in a specially constructed high-speed stirring apparatus. The apparatus consisted of a Stir-o-vac[20] high-speed stirrer powered by a 10 000-rpm motor. The bearing of the stirrer had an O-ring seal for the center hole of a three-necked Pyrex flask and a Teflon

[16] N. F. Mott, Proc. Cambridge Phil. Soc. 32, 281 (1936).
[17] J. Friedel, Phil. Mag. 43, 153 (1952).
[18] Foote Mineral Co., Exton, Pa.
[19] A. D. McKay Co., N. Y.
[20] Labline Co., Melrose Park, Ill.

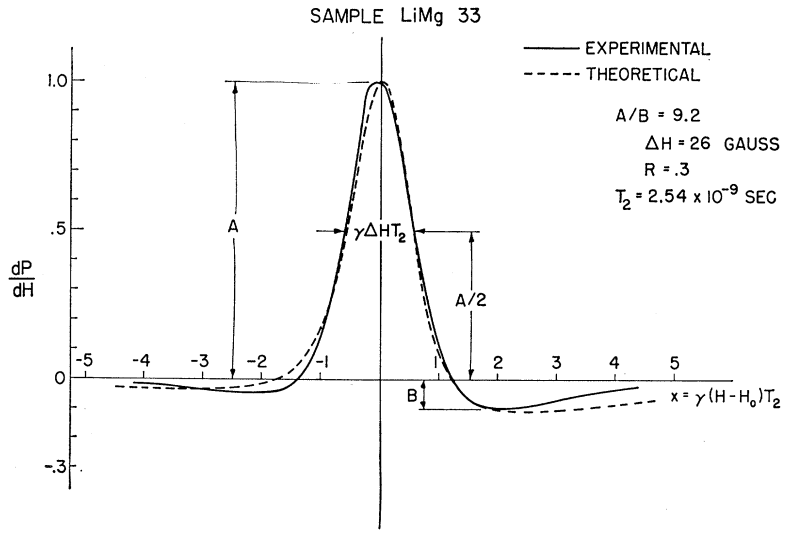

FIG. 2. Experimental and theoretical CESR line shape for a lithium-magnesium alloy having a concentration of 1.3% Mg.

seal for the stainless-steel stirring rod. The two other holes in the flask were used for a thermometer and for argon flushing.

The dispersions were made in mineral oil heated to 250°C. Predegassing of the mineral oil enabled it to withstand the high temperature without noticeable carburization. The heat was supplied by an electric heating mantle on the bottom of the flask. The dispersing was done under a 99.999% argon atmosphere. The materials for a typical dispersion consisted of 100 cc of mineral oil, 10 cc of alkali metal or alloy, and about 0.35 cc of oleic acid. The latter served the purpose of preventing coagulation, as suggested by Schumacher and Vehse.[21]

The procedure is to heat the mixture to 250°C, turn on the stirrer for 10 min, and then cool rapidly to room temperature by removing the mantle and directing forced cool air on the flask with the stirrer still operating. The dispersion is concentrated to a filling factor of almost 100% by centrifuging. Molten paraffin is then added to reduce the filling factor to about 50%. The hot dispersion is allowed to solidify in a 4-mm Pyrex tube, which is then broken off to a length of 1 cm. The ends of the sample tube are sealed with pure paraffin.

C. Molten-State Measurements

The usual procedure was to measure the CESR of a sample within a few hours of preparation and certainly no later than one day after. The measurements made at 77°K agreed with those made at 300°K when the temperature-broadening effect was taken into account.

The molten-state measurements were performed on several *Li*Sn and *Li*Pb alloys. In these experiments Kevin Cornell assisted. He has subsequently extended them to study impurities *only* soluble in the molten host.

[21] R. T. Schumacher and W. E. Vehse, J. Phys. Chem. Solids 24, 297 (1963).

There were two reasons for doing molten-state measurements. The first was to investigate possible experimental effects regarding the anomalous drop in the spin-flip cross sections at Sn and Pb. The second was to study a sharp decrease in linewidth noticed in certain samples upon remeasurement several weeks after fabrication. The systems that showed the most deterioration were *Li*Sn and *Li*Pb. The aged linewidths were about 1 G, even though the initial linewidths ranged from 20 to 86 G. *Li*Ag, *Li*Au, *Na*Cd, *Na*Sn, and *Na*Tl all showed a decrease of linewidth of less than a factor of $\frac{1}{2}$. The remainder of the alloy systems exhibited practically no change in linewidth with aging.

To accomplish these measurements, the EPR cavity was modified so that it could be resistance-heated to a temperature of 250°C. The samples consisted of the dispersed alloy particles completely sealed in glass tubes. The samples were supported in the cavity by a quartz tube.

Heating the samples into the molten state caused the original linewidths to reappear, within experimental

TABLE I. Relevant physical properties of lithium and sodium (T=300°K).

	Li	Na
Lattice type	bcc	bcc
Lattice constant a (Å)	3.50	4.28
Wigner-Seitz radius r_0 (Å)	1.72	2.10
k_F (a.u.)[a]	0.579	0.482
m_b/m_0[a]	1.32	1.00
$\rho_b(E_F)$ (erg^{-1} cm^{-3})	1.22×10^{34}	7.55×10^{33}
m_t/m_0[a]	2.0	1.4
$\rho_t(E_F)$ (erg^{-1} cm^{-3})	1.87×10^{34}	1.06×10^{34}
N_0 (cm^{-3})	4.67×10^{22}	2.55×10^{22}
Conductivity σ (sec^{-1})	1.1×10^{17}	2.1×10^{17}
Skin depth δ at $f=9\times10^9$ cps (μ)	1.55	1.10
Spin penetration depth δ_s (μ)	17	11
Mean free path Λ (Å)	110	350
Fermi velocity v_F (cm/sec)	1.31×10^8	1.07×10^8

[a] F. S. Ham, Phys. Rev. 128, 82 (1962); 128, 2524 (1962).

error. For example, for a *Li*Sn alloy, the initial linewidth was 26 G, the aged ΔH was 3 G, the molten state ΔH was 31 G, and the linewidth of the freshly cooled sample was 29 G. Similar results were obtained for two *Li*Pb samples.

We thus conclude that our method of sample preparation quenches in a nonequilibrium concentration of impurities for the alloy systems mentioned above. Aging of the samples allows precipitation of the impurities or perhaps formation of a second phase. However, since a linear ΔH-versus-c relation was obtained over all the experimental range for all alloys that deteriorated, except *Li*Sn and *Na*Sn, and since for these two alloys the initial slope could be determined reproducibly, we believe that the cross sections for our alloys represent true random solid solutions.

D. Line Shape

Dyson[22] has calculated the paramagnetic contribution to the surface impedance of a metallic sample in the neighborhood of CESR. Three simplifying assumptions were made: (a) The conduction electrons were taken to be an isotropic gas of noninteracting electrons colliding with impurities and moving under the influence of applied electric and magnetic fields; (b) the applied magnetic field $\mathbf{H}_0$ was assumed normal to the surface of the sample, taken to be a flat metal plate; and (c) normal skin-effect conditions prevail.

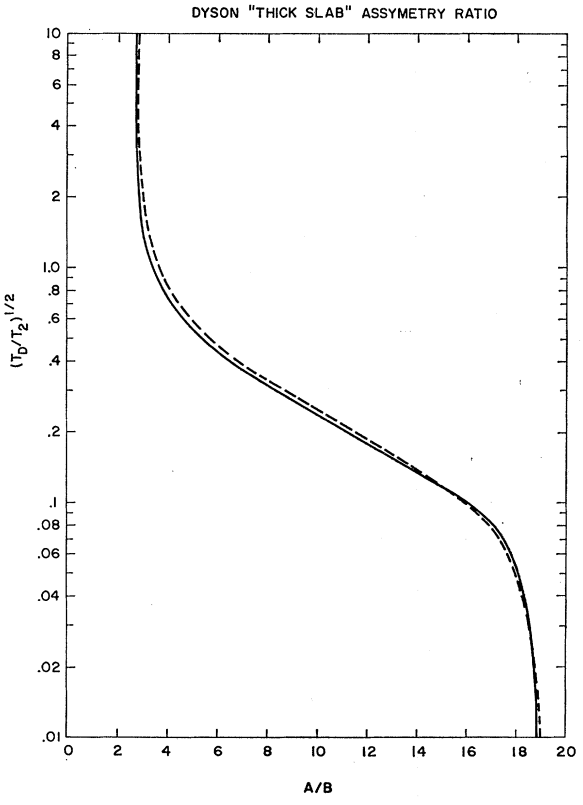

FIG. 3. Dyson line-shape parameter A/B for the thick-slab case as a function of $(T_D/T_2)^{1/2}$. The solid line was obtained in the present work, while the dashed line was obtained by Feher and Kip.

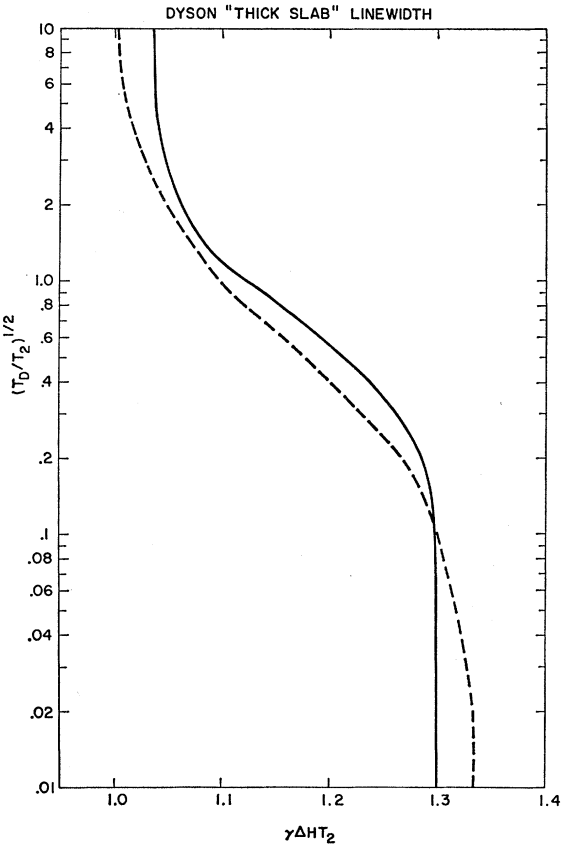

FIG. 4. Dyson line-shape parameter $\gamma\Delta HT_2$ for the thick-slab case as a function of $(T_D/T_2)^{1/2}$. The solid line was obtained in the present work, while the dashed line was obtained by Feher and Kip.

Because our particle sizes were not in Dyson's "thick-slab" regime (particle size$\gg$skin depth δ), a comparison between theory and experiment required the knowledge of the exact particle distributions of the Li-alloy and Na-alloy dispersions. We measured the distributions for a typical pure-Li and a pure-Na dispersion. For both dispersions, the distributions were approximately Gaussian and the particles appeared spherical. Let $\bar{D}$ be the average particle diameter; σ, the rms width of the distribution; and δ, the skin depth of the pure metal at 300°K and 9 Gc/sec. For the Li dispersion, $\bar{D}=25\ \mu$, $\sigma=11\ \mu$, and $2\delta=3.1\ \mu$. For the Na dispersion, $\bar{D}=7.8\ \mu$, $\sigma=4.2\ \mu$, and $2\delta=2.2\ \mu$.

A computer program was written to evaluate Dyson's general expression for the surface impedance [Eqs. (71) and (77) of his paper]. We have taken Dyson's parameter λ (defined as θ/δ, where θ is the thickness of

[22] F. J. Dyson, Phys. Rev. 98, 349 (1955); see also Feher and Kip (Ref. 3).

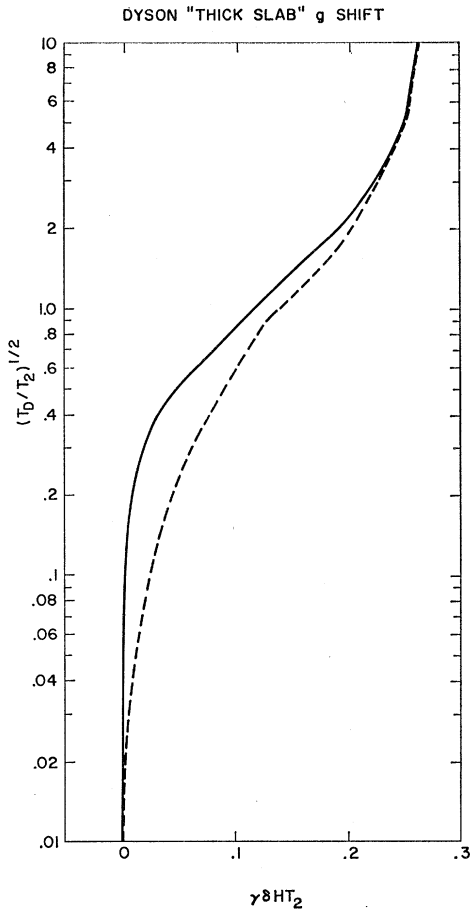

FIG. 5. Dyson line-shape parameter $\gamma\delta HT_2$ for the thick-slab case as a function of $(T_D/T_2)^{1/2}$. The solid line was obtained in the present work, while the dashed line was obtained by Feher and Kip.

the plate) to be $D/2\delta$, where D is a given particle diameter. Only the resonant part of the surface impedance was retained. The program averaged the Dyson line shape over the measured particle distribution. Since D is generally much larger than δ, the distribution was weighted by D^2, which accounts for the fact that a bigger particle produces a larger signal than a smaller one. The computer program calculated the derivative of the power absorption, which is proportional to the real part of the surface impedance. We also calculated the three fundamental line-shape parameters A/B, $\gamma\Delta HT_2$, and $\gamma\delta HT_2$. γ is the electron magnetogyric ratio. On the first derivative line shape, A is the amplitude of the low-field peak, while B is the amplitude of the high-field peak. A/B is called the asymmetry ratio, while δH is the distance to the right from the low-field A peak of the exact resonance position. The linewidth ΔH and peak shift δH are multiplied by γT_2 to produce a dimensionless quantity.

We measured A/B and ΔH for each sample but made no measurements of δH.[23] Figure 2 shows experimental and theoretical line-shape derivatives for a LiMg alloy having a concentration of 1.3% Mg, $\Delta H=26$ G, and $A/B=9.2$. Figure 2 also illustrates the meaning of the parameters A, B, and $\gamma\Delta HT_2$. The only adjustment is in the amplitude normalization. The agreement is excellent, except in the tails. The parameter R is defined as

$$R=(T_D/T_2)^{1/2}, \tag{39}$$

where T_D is the time necessary for a Fermi electron to diffuse a distance equal to the skin depth. The formula for T_D is

$$T_D=3\delta^2/2v_F\Lambda, \tag{40}$$

where v_F is the Fermi velocity and Λ is the mean free path. The spin diffusion depth δ_s is defined as the distance a Fermi spin diffuses before its spin is flipped:

$$\delta_s=(\tfrac{2}{3}v_F\Lambda T_2)^{1/2}. \tag{41}$$

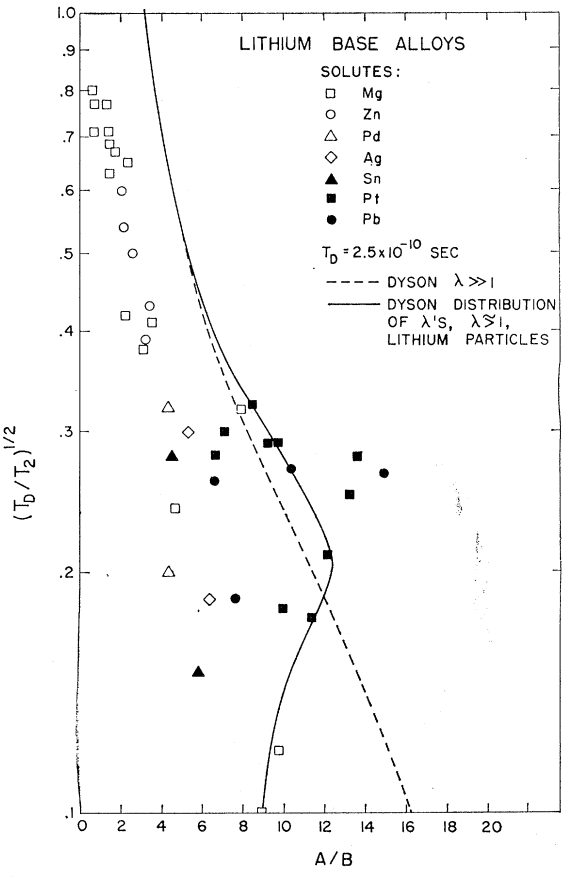

FIG. 6. Experimental and theoretical asymmetry ratios for lithium-base alloys. The ordinate is Dyson's parameter R, while the abscissa is A/B. The solid curve is for the measured lithium particle distribution, while the dashed curve is the thick-slab theory T_D as given by Eq. (40).

[23] Measurements of δH result in values of the impurity-induced g shift. The first such measurements have been reported by Hahn and Enderby (Ref. 12).

Table I gives a summary of some useful physical properties of lithium and sodium. In the table, m_b/m_0 is the band effective-mass ratio and $\rho_b(E_F)$ is the density of states at E_F derived from the value of m_b. These are the quantities we have used in calculating T_1. For reference, in Table I we also give values for the phonon-enhanced thermal effective-mass ratio (m_t/m_0) and for the thermal density of states $\rho_t(E_F)$. In addition, we give the number density of electrons N_0 and the Fermi wave vector k_F.

As one test of our line-shape program, the three line-shape parameters for the thick-slab limit ($\lambda \gg 1$) were calculated as a function of R so that comparison could be made with the Feher and Kip[3] graphical evaluation of Dyson's equations. This comparison is shown in Figs. 3–5. There is excellent agreement for A/B, but exact quantitative agreement is lacking for $\gamma\Delta HT_2$ and $\gamma\delta HT_2$. We believe our computer evaluation to be more accurate than the original graphical evaluation.

Figures 6 and 7 show the comparison between the measured asymmetry ratios A/B for lithium-base and sodium-base alloys, respectively, and the predictions of Dyson's theory. Figure 6 also shows a comparison with the thick-slab theory. One can draw a number of conclusions. The first is that the large scatter in the experimental asymmetry values indicates a sensitivity

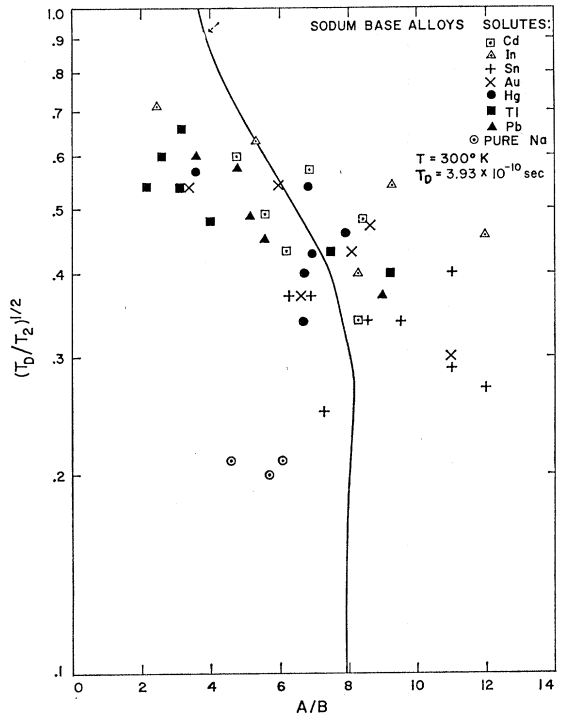

FIG. 7. Experimental and theoretical asymmetry ratios for sodium-base alloys. The ordinate is Dyson's parameter R, while the abscissa is A/B. The solid curve is for the measured sodium particle distribution. For best fit T_D was chosen larger than that given by Eq. (40) ($T_D = 4.9\times10^{-11}$ sec). This was attributed to the presence of impurities in the sodium.

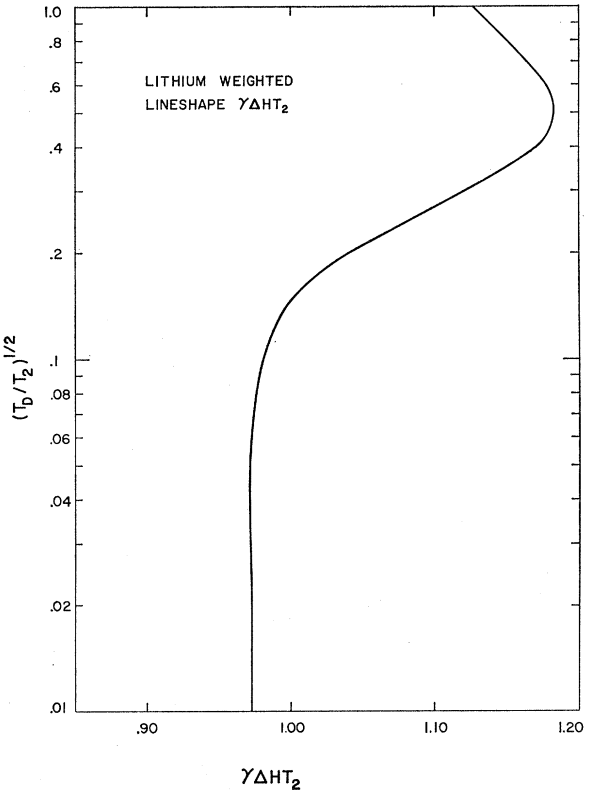

FIG. 8. R versus $\gamma\Delta HT_2$ for the lithium particle distribution.

to the details of sample preparation. For a given ΔH, the scatter in A/B is much larger than that in ΔH itself. The theory is in general agreement with the data, although the lithium-alloy asymmetries consistently lie below the Dyson theory, and even lie below the minimum predicted value of 2.7.

Figure 8 shows the relationship between ΔH and T_2 as a function of R for the lithium particle distribution. The behavior for the sodium particle distribution is quite similar. From Figs. 6 and 7 we see that the values of R ranged from 0.15 to 0.8. The relation between ΔH and T_2 is seen to range between $\gamma\Delta HT_2 = 1.000$ and $\gamma\Delta HT_2 = 1.175$. For consistency and convenience, all calculations in this paper use the conversion

$$\gamma\Delta HT_2 = 1.100. \tag{42}$$

This is in error by $\pm 10\%$ at most, which is approximately the same as the error in measuring ΔH.

IV. EXPERIMENTAL RESULTS AND DISCUSSION

A. Relation between σ and $\partial\Delta H/\partial c$

In the following paragraph we relate the broadening factor $\partial\Delta H/\partial c$ to the spin-flip scattering cross section σ. Only electrons near the Fermi surface can change their spin state. Let us introduce the concept of spin mean free path l_s, which is the length of path traveled by a conduction electron before its spin state is reversed

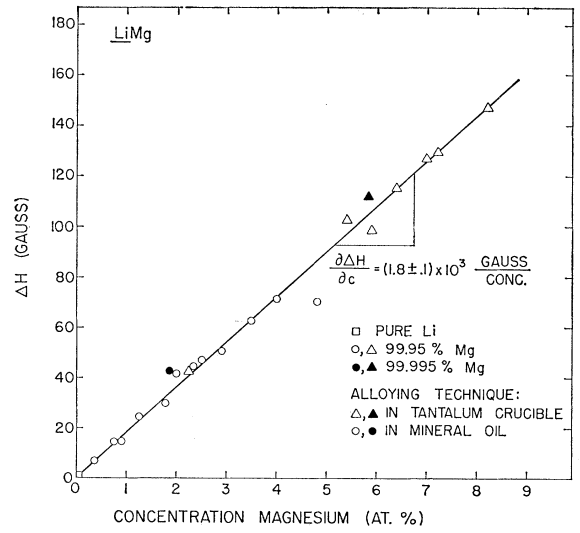

FIG. 9. Dependence of the CESR linewidth ΔH on concentration c for *Li*Mg alloys.

by interaction with the spin-dependent potential of an impurity atom:

$$l_s = 1/N_0 c\sigma. \tag{43}$$

N_0 is the number of host atoms per cm³, and c is the fractional concentration of impurity atoms. But we also have

$$l_s = v_F T_1 = 1.1 v_F/\gamma\Delta H. \tag{44}$$

Combining Eqs. (43) and (44), we obtain the result

$$\sigma = (\gamma/1.1 N_0 v_F)\partial\Delta H/\partial c. \tag{45}$$

In Eq. (45) we have introduced the partial derivative because we are only interested in the increase in linewidth due to added impurities. Table I gives N_0 and v_F for lithium and sodium.

B. Experimental Procedure

Figures 9–16 show samples of our experimental data for ΔH versus c. Except for *Li*Mg, *Li*Tl, and *Na*Pb,

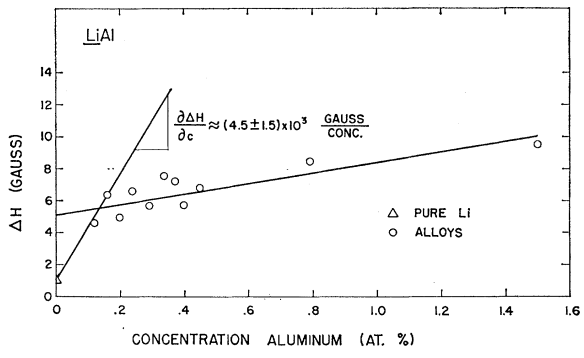

FIG. 10. Dependence of the CESR linewidth ΔH on concentration c for *Li*Al alloys.

TABLE II. Experimental values of the broadening factor for lithium-base alloys. NS means not soluble; no broadening observed. IS means initial slope; saturation observed.

Impurity	Z	$\partial\Delta H/\partial c$ [G/(unit conc.)]
Mg	12	$(1.79\pm0.09)\times10^3$
Al	13	$(4.5\ \pm1.5\ )\times10^3$ (IS)
Cu	29	NS
Zn	30	$(1.86\pm0.09)\times10^5$
Ga	31	$(4.10\pm0.20)\times10^5$
Ge	32	NS
Pd	46	$(5.7\ \pm0.7\ )\times10^5$ (IS)
Ag	47	$(9.65\pm0.50)\times10^5$
Cd	48	$(2.12\pm0.12)\times10^6$
In	49	$(2.85\pm0.15)\times10^6$
Sn	50	$(6.1\ \pm0.7\ )\times10^5$ (IS)
Sb	51	NS
Pt	78	$(7.0\ \pm0.8\ )\times10^6$ (IS)
Au	79	$(1.87\pm0.30)\times10^7$
Hg	80	$(2.99\pm0.12)\times10^7$
Tl	81	$(2.53\pm0.19)\times10^7$
Pb	82	$(4.6\ \pm0.5\ )\times10^6$
Bi	83	NS

we have omitted the data for which a linear dependence of ΔH on c was observed. In the cases of *Li*Al, *Li*Pd, *Li*Sn, *Li*Pt, and *Na*Sn, a definite saturation in ΔH occurs. The saturation in the *Li*Al alloys occurs at a concentration of 0.1% Al. A similar behavior was previously seen by MacDonald[24] in thermoelectric measurements. Because of the dilute nature of these alloys, we have not made an effort to determine experi-

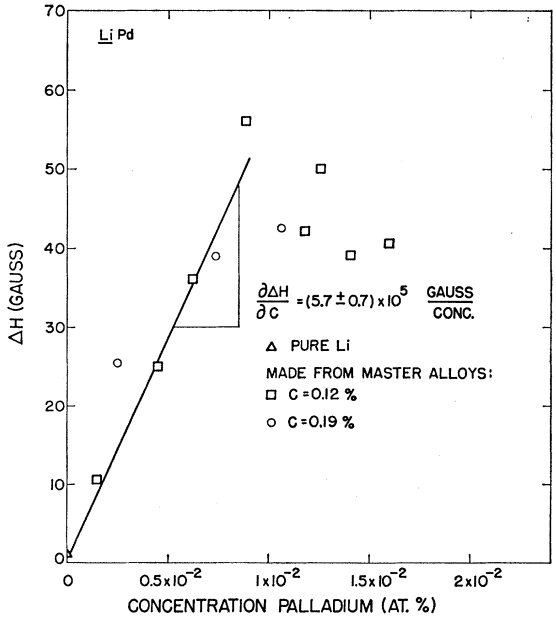

FIG. 11. Dependence of the CESR linewidth ΔH on concentration c for *Li*Pd alloys.

[24] D. K. C. MacDonald *et al.*, Phil. Mag. **6**, 1431 (1961).

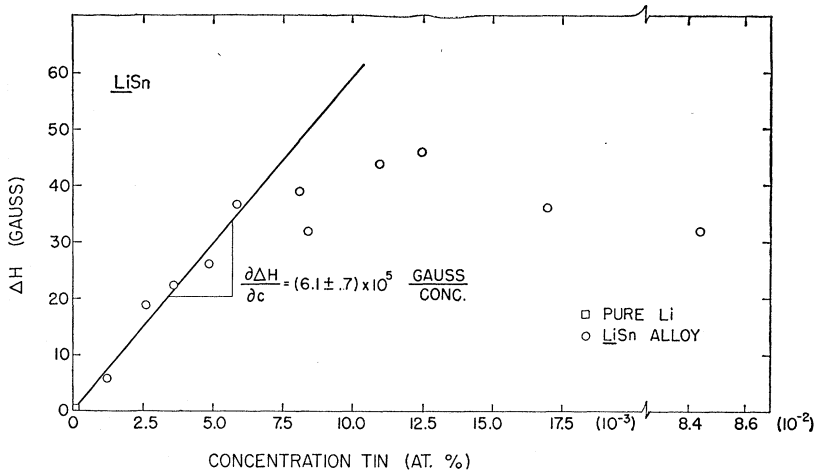

FIG. 12. Dependence of the CESR linewidth ΔH on concentration c for *Li*Sn alloys.

mentally the microscopic nature of this saturation. All we can say is that in these systems one has a random solution solubility limit, probably due to precipitation of the impurity atoms or to formation of a second phase. For the impurities with the highest Z, we observe that the CESR linewidth is sensitive to concentrations of impurity as low as 1 atom in 10^7 (e.g., *Na*Tl alloys). On the other hand, for the *Li*Mg alloys, concentration as large as 10% failed to produce noticeable nonlinearity between ΔH and c.

Tables II and III summarize the experimental results in terms of the broadening factors $\partial\Delta H/\partial c$ for the lithium-base and sodium-base alloys, respectively. For most alloy systems ΔH versus c is linear, so that the broadening factor is simply the slope of the line. Where saturation occurred, the broadening factor was taken to be the initial slope of the ΔH-versus-c plot. The errors are estimated from the scatter in the data.

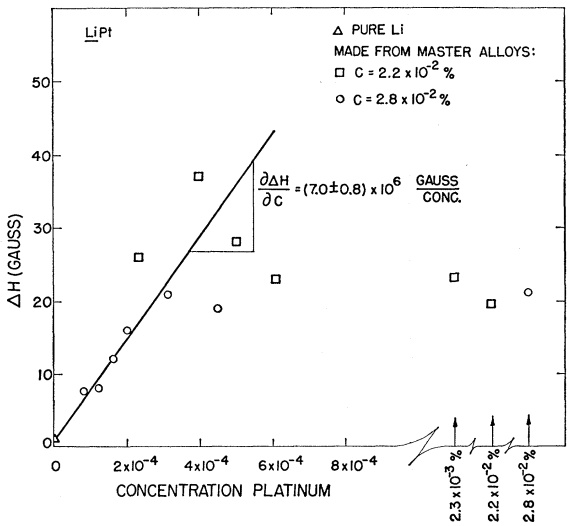

FIG. 13. Dependence of the CESR linewidth ΔH on concentration c for *Li*Pt alloys.

Tables II and III also list several elements found to be insoluble in lithium and sodium.

The broadening factors cover a range of five orders of magnitude. From Eq. (45) we find that the spin-flip cross sections range from approximately 10^{-21} cm^2 for Mg in Li to 10^{-16} cm^2 for Hg in Li or Na. Since 10^{-16} cm^2 is roughly the same as the unitarity limit for spin-flip scattering (approximately 5×10^{-16} cm^2 for Li and Na), the spin-flip events are highly probable when a Fermi electron collides with a Hg impurity atom, but they only have a probability of about 10^{-5} when a collision occurs with a Mg impurity atom. This large range of magnitude is related to the large variation in spin-orbit splitting of free atoms.

The valence dependence of the experimental cross sections in the gold and silver rows is shown in Figs. 17–21. The cross sections have a nonmonotonic valence dependence; they generally increase as the valence difference increases. But there is a consistent leveling off and then decrease for valence differences of +2 and +3. This behavior is in sharp contrast to the

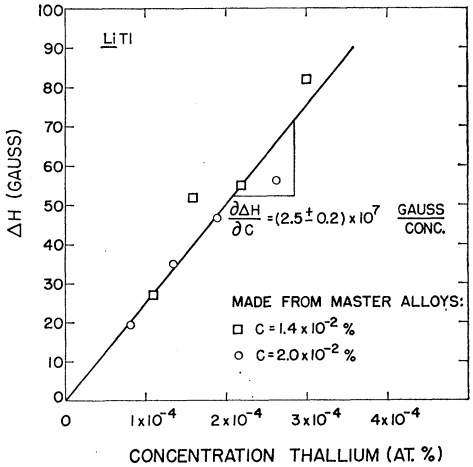

FIG. 14. Dependence of the CESR linewidth ΔH on concentration c for *Li*Tl alloys.

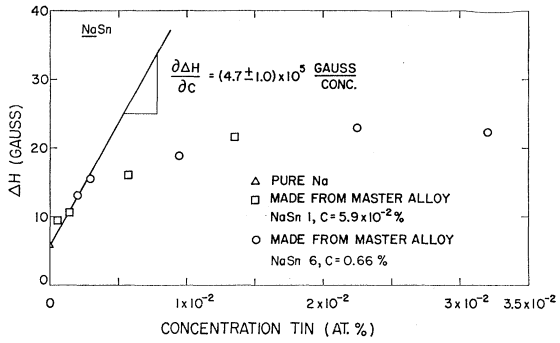

FIG. 15. Dependence of the CESR linewidth ΔH on concentration c for *Na*Sn alloys.

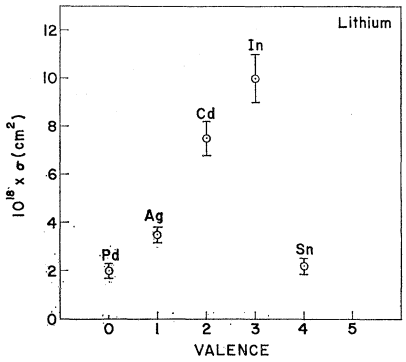

FIG. 17. Spin-flip cross section in lithium: silver-row impurities.

momentum scattering cross section of nontransition-metal impurities, which is proportional to the residual resistivity per impurity atom. This cross section varies by Z_v^2 (Linde's rule), where Z_v is the valence difference between the impurity atom and the host, for impurities with Z_v as large as +4 dissolved in the noble metals.[25]

Linde's rule is obeyed by the spin-flip cross sections for small positive (+1 and +2) valence differences. However, there are two observed departures. One is the leveling off and decrease in $\sigma_{\text{spin-flip}}$ for Z_v equal to +2 and +3. The other departure relates to the cross sections of Pd and Pt. Linde's rule would predict these cross sections to be approximately the same as those for Cd and Hg, respectively. However, the observed cross sections are smaller than those for Ag and Au, respectively.

C. Comparison of Monovalent-Impurity Results with Theory

In order to compare the experimental cross sections with theory, the overlap integrals a_{nl} between plane waves and nl core states were calculated numerically using FORTRAN coding on an IBM 7094 computer. The Hartree-Fock-Slater (HFS) wave functions of Herman and Skillman[26] were used for the core states. The contributions from all p and d core orbitals were examined for a number of cases, and it was found that the largest contribution (better than 95%) to $\langle V_1^2 \rangle_F$ comes from overlap with the p orbital immediately below the valence state of the impurity. Simpson's rule, modified for unequal intervals, was used to compute the overlap integrals a_{np} between plane waves and the HFS core functions. The wave-function intervals used were those in the Herman-Skillman tabulation. Table IV shows the spin-orbit splittings Δ_{nl} for p and d states just below the valence states. These splittings were obtained from x-ray spectra tables.

For p and d core states, one obtains the coupling constants λ using the relations

$$\lambda_{np} = \tfrac{2}{3}\Delta_{np} \quad \text{and} \quad \lambda_{nd} = \tfrac{2}{5}\Delta_{nd}.$$

For a given n, the overlap integrals with p and d orbitals are about the same, but since the splittings

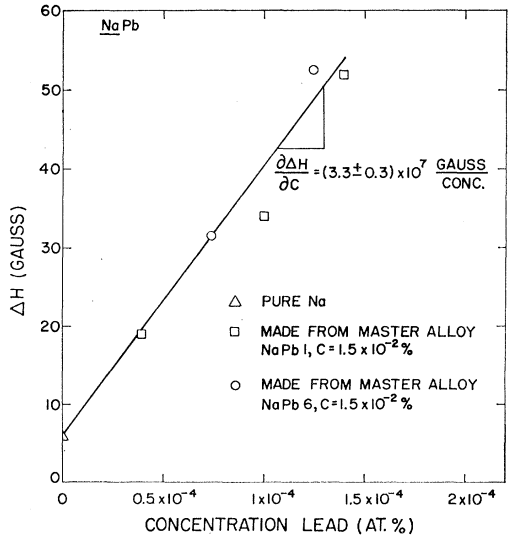

FIG. 16. Dependence of the CESR linewidth ΔH on concentration c for *Na*Pb alloys.

TABLE III. Experimental values of the broadening factor for sodium-base alloys. NS means not soluble; no broadening observed. IS means initial slope; saturation observed.

Impurity	Z	$\partial \Delta H/\partial c$ [G/(unit conc.)]
Zn	30	NS
Ga	31	NS
Ag	47	NS
Cd	48	$(1.08 \pm 0.12) \times 10^6$
In	49	$(3.86 \pm 0.30) \times 10^6$
Sn	50	$(4.7 \pm 1.0) \times 10^5$ (IS)
Pt	78	NS
Au	79	$(4.9 \pm 0.4) \times 10^6$
Hg	80	$(1.58 \pm 0.22) \times 10^7$
Tl	81	$(4.50 \pm 0.35) \times 10^7$
Pb	82	$(3.3 \pm 0.3) \times 10^7$

[25] J. M. Ziman, *Electrons and Phonons* (Clarendon Press, Oxford, 1962), p. 340.
[26] F. Herman and S. Skillman, *Atomic Structure Calculations* (Prentice-Hall, Inc., Englewood Cliffs, N. J., 1963).

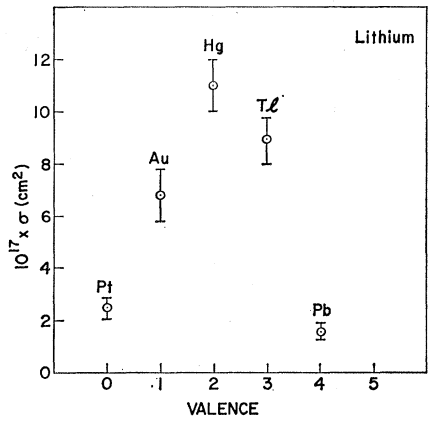

FIG. 18. Spin-flip cross section in lithium: gold-row impurities.

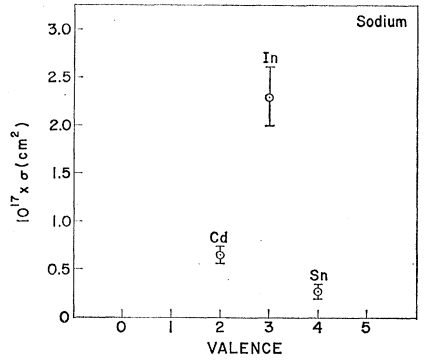

FIG. 19. Spin-flip cross section in sodium: silver-row impurities.

are much larger for the p states, they have the major contribution to the matrix elements. We have, in fact, neglected all contributions except those from the p states in the calculations presented in this paper.

In Table V[27] we give the comparison between the experimental and theoretical σ's for monovalent impurities in lithium and sodium. The OPW cross sections agree with experiment within a factor of 2.2 despite the fact that the experimental σ's cover a range of 20. These data were the only data obtained on monovalent impurities, since we found Cu to be insoluble in Li, and Ag to be insoluble in Na. The insolubility was established by looking for the line-broadening effect on the CESR of "alloys" having nominal concentrations up to approximately 1 at.% (see Tables II and III).

TABLE IV. Core-state spin-orbit splittings Δ_{nl}.[a]

Element	Δ_{nl} (eV)	
Mg ($3s^2$)	0.18 ($2p$)	
Al ($3s^23p$)	0.40 ($2p$)	
Cu ($4s$)	2.8 ($3p$)	0.25 ($3d$)
Zn ($4s^2$)	2.5 ($3p$)	0.34 ($3d$)
Ga ($4s^24p$)	4.0 ($3p$)	0.40 ($3d$)
Pd ($5s^0$)	6.1 ($4p$)	
Ag ($5s$)	7.0 ($4p$)	0.55 ($4d$)
Cd ($5s^2$)	7.9 ($4p$)	0.70 ($4d$)
In ($5s^25p$)	9.1 ($4p$)	0.70 ($4d$)
Sn ($5s^25p^2$)	10.2 ($4p$)	0.55 ($4d$)
Pt ($6s^0$)	13.6 ($5p$)	
Au ($6s$)	18 ($5p$)	1.52 ($5d$)
Hg ($6s^2$)	21 ($5p$)	1.86 ($5d$)
Tl ($6s^26p$)	23.4 ($5p$)	2.20 ($5d$)
Pb ($6s^26p^2$)	24.3 ($5p$)	2.60 ($5d$)

[a] Landolt-Börnstein, *Zahlenwerte und Funktionen* (Springer-Verlag, Berlin, 1950), Vol. I, Part 1; A. E. Sandström, *Encyclopedia of Physics* (Springer-Verlag, Berlin, 1957), Vol. 30.

[27] Because of an error, the values of σ_{theor} for the impurities reported in the preliminary account of this work in Ref. 1 were incorrect by a small numerical factor. The corrected values are given in this paper.

D. Comparison of Nonmonovalent-Impurity Results with Theory

Equation (38) was numerically integrated by computer, using Milne's method.[28] The starting values for the numerical integration were obtained by a power-series solution near $r=0$. The screening parameter α was determined in the following manner: For each value of Z_v, the s-, p-, and d-wave phase shifts η_0, η_1, and η_2 were computed for several values of α. The optimum value of α was that for which η_0, η_1, and η_2 satisfied the Friedel sum rule[17]

$$Z_v=-\frac{2}{\pi}\sum_{l=0}^{\infty}(2l+1)\eta_l. \tag{46}$$

For $Z_v=0$, the solution to Eq. (38) is just $rj_l(k_Fr)$. At large distances, $r\gg\alpha^{-1}$, this function varies sinus-

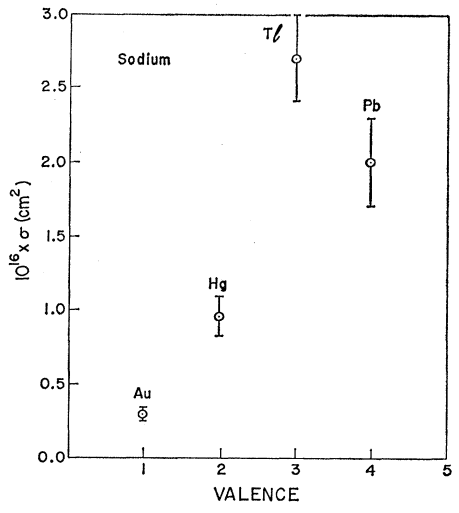

FIG. 20. Spin-flip cross section in sodium: gold-row impurities.

[28] K. S. Kunz, *Numerical Analysis* (McGraw-Hill Book Co., New York, 1957), p. 202.

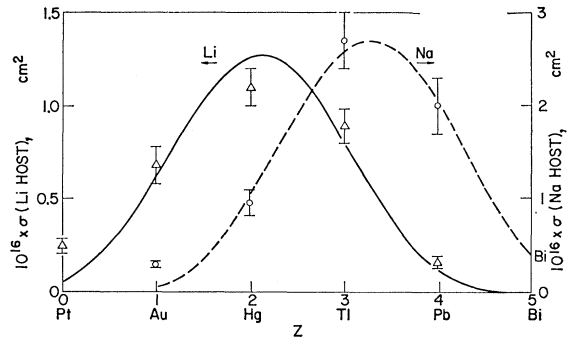

FIG. 21. Resonance-theory fit to gold-row impurities spin-flip cross section in lithium (left axis) and sodium (right axis). After Ferrell and Prange (Ref. 32).

oidally. The phase shifts were determined by comparing the asymptotic solution of Eq. (38) for $Z_v \neq 0$ with the asymptotic form of $rj_l(k_F r)$. The step lengths in the integration were chosen sufficiently small, so that a halving of the step length produced negligible change in the phase shift.

Tables VI and VII summarize the results of these calculations. The optimum screening parameters and the phase shifts for a screened Coulomb potential in lithium and sodium are given. Except for $Z_v = -1$, the values of $\alpha(k_F)$ do not depend strongly on Z_v and are close to the values of α_{TF} given by the Thomas-Fermi-Mott screening approximation. The screened Coulomb functions ϕ_p were normalized at large distances to the same amplitude as a plane wave, since a scattering potential of finite range can produce only a phase shift at large distances. The phase shifts were measured at $k_F r > 15$. The effect of screening, in our simple model, is to produce larger overlap integrals with core functions than a plane wave for attractive potentials ($Z_v > 0$), and smaller overlap integrals for repulsive potentials ($Z_v < 0$).

The experimental and theoretical spin-flip cross sections for nonmonovalent impurities in Li and Na are shown in Table VIII. For Pd and Pt (which present repulsive potentials) and the group-IB or -IIB elements, the simple OPW procedure gives excellent account of the results over a range of 10^5 in experimental values. This agreement demonstrates convincingly that (a) the mechanism of spin flip is impurity-induced spin-orbit coupling and (b) that a valence effect of the type discussed is operative. However, the large discrepancy with the group-IVA elements and the similar though less marked effect for the group-IIIA elements indicates a breakdown of our simple theory for large valence differences.

TABLE V. Experimental and theoretical spin-flip scattering cross sections for monovalent impurities in lithium and sodium.

Alloy	σ_{expt} (cm²)	σ_{theor} (cm²)
*Li*Ag	$(3.5\pm0.3)\times10^{-18}$	3.0×10^{-18}
*Li*Au	$(6.8\pm1.0)\times10^{-17}$	3.6×10^{-17}
*Na*Au	$(2.9\pm0.3)\times10^{-17}$	1.3×10^{-17}

TABLE VI. Optimum screening parameters and phase shifts for a screened Coulomb potential in *lithium*.

Valence difference Z_v	−1	0	1	2	3
Impurities			Mg Zn	Al Ga	
	Pd Pt	Ag Au	Cd Hg	In Tl	Sn Pb
Phase shifts					
η_0	−0.688	0	1.245	2.453	3.241
η_1	−0.198	0	0.093	0.195	0.434
η_2	−0.057	0	0.012	0.020	0.035
Optimum screening parameter (units of $k_F = 0.579$ a.u.)					
$\alpha(k_F)$	1.22	···	1.90	1.99	1.95
$\alpha_{TF} = 2.11 k_F = 1.22$ a.u.					

TABLE VII. Optimum screening parameters and phase shifts for a screened Coulomb potential in *sodium*.

Valence difference Z_v	−1	0	1	2	3
Impurities			Cd	In	Sn
		Au	Hg	Tl	Pb
Phase shifts					
η_0		0	1.342	2.605	3.448
η_1		0	0.067	0.157	0.380
η_2		0	0.007	0.013	0.024
Optimum screening parameter (units of $k_F = 0.482$ a.u.)					
$\alpha(k_F)$		···	2.26	2.29	2.22
$\alpha_{TF} = 1.88 k_F = 0.905$ a.u.					

Table IX shows a comparison between a portion of our experimental results and the only data available from other workers at this time. There is satisfactory agreement with the Hahn-Enderby[12] data, but a factor of 2 discrepancy with the Garif'ianov-Starikov[12] result.

E. Discussion

We have seen that the effect of nonmagnetic impurities on the CESR in lithium and sodium is appreciable. The strength of the interaction is conveniently discussed in terms of the spin-flip scattering cross section of the impurities for conduction electrons. The magnitude of this cross section varies roughly as λ^2, where λ is the effective spin-orbit coupling constant of the impurity atom when dissolved in the host metal. The preponderance of the data for low-valence impurities is adequately explained by an elementary theory in which the spin-orbit interaction is taken as a perturbation, and screening is taken into account in the Thomas-Fermi approximation. However, for the high-valence impurities ($Z = 3,4$) in the silver and gold rows, an anomalous resonantlike behavior in the cross section is found which cannot be explained by our theory.

Recently, Vassel[29] found that selenium impurities in copper produced a small value of the residual re-

[29] C. R. Vassal, J. Phys. Chem. Solids **7**, 90 (1958).

sistivity than arsenic. Coqblin *et al.*[30] studied the resistivity and thermoelectric power of silver-base alloys containing selenium and krypton. When combined with previous data, the valence dependence of the resistivity of copper-row (Cu-Kr) impurities in silver has a resonant shape with a peak at arsenic. The thermoelectric power behaves anomalously, going to zero between arsenic and selenium. Friedel[31] has interpreted the nonmonotonic behavior in resistance as due to a scattering resonance with a virtual bound p state.

We have pointed out[1] that the spin-flip scattering cross section is best discussed in terms of phase shifts in a j,l representation, where j is the total angular momentum (spin plus orbit of an individual electron) and thus equal to either $l+\frac{1}{2}$ or $l-\frac{1}{2}$. Thus, if only p waves are important, then

$$\sigma_{\text{spin-flip}}=(8\pi/3k_F^2)\sin^2(\eta_{3/2}{}^1-\eta_{1/2}{}^1), \qquad (47)$$

where $\eta_j{}^l$ is the phase shift of the j,l partial wave. For $\sigma_{\text{spin-flip}}$ to go through a maximum,[1] the sine must either go to unity (corresponding to the unitarity limit for $\sigma_{\text{spin-flip}}$) or the argument of the sine must go through a maximum.[1] Since none of the cross sections achieves the unitarity limit, there must be a maximum in the argument. We have published results[1] of a procedure different from that described in this paper for computing the phase shifts. We give a more detailed account in paper II of this series. It indeed shows a maximum in the argument of the sine, but the maximum occurs for the s^2p^3 atomic configuration. This corresponds, in fact, to Friedel's proposal[31] to account for residual resistivity.

TABLE VIII. Experimental and theoretical spin-flip scattering cross sections for impurities having a valence difference $V-1$ with respect to lithium and sodium.

Alloy	$V-1$	σ_{expt} (cm^2)	σ_{theor} (cm^2)
*Li*Mg	+1	$(6.4\pm0.5)\times10^{-21}$	0.92×10^{-21}
*Li*Al	+2	$(1.6\pm1.0)\times10^{-20}$	4.9×10^{-21}
*Li*Zn	+1	$(6.8\pm0.6)\times10^{-19}$	0.98×10^{-19}
*Li*Ga	+2	$(1.5\pm0.1)\times10^{-18}$	5.2×10^{-19}
*Li*Pd	−1	$(2.0\pm0.3)\times10^{-18}$	0.78×10^{-18}
*Li*Cd	+1	$(7.5\pm0.7)\times10^{-18}$	6.2×10^{-18}
*Li*In	+2	$(1.0\pm0.1)\times10^{-17}$	1.7×10^{-17}
*Li*Sn	+3	$(2.2\pm0.3)\times10^{-18}$	1.3×10^{-16}
*Li*Pt	−1	$(2.5\pm0.4)\times10^{-17}$	0.65×10^{-17}
*Li*Hg	+1	$(1.1\pm0.1)\times10^{-16}$	0.85×10^{-16}
*Li*Tl	+2	$(8.9\pm0.9)\times10^{-17}$	2.2×10^{-16}
*Li*Pb	+3	$(1.6\pm0.3)\times10^{-17}$	0.98×10^{-15}
*Na*Cd	+1	$(6.6\pm0.8)\times10^{-18}$	2.5×10^{-18}
*Na*In	+2	$(2.3\pm0.3)\times10^{-17}$	0.75×10^{-17}
*Na*Sn	+3	$(2.8\pm0.6)\times10^{-18}$	0.82×10^{-16}
*Na*Hg	+1	$(9.6\pm1.5)\times10^{-17}$	3.1×10^{-17}
*Na*Tl	+2	$(2.7\pm0.3)\times10^{-16}$	0.97×10^{-16}
*Na*Pb	+3	$(2.0\pm0.3)\times10^{-16}$	7.1×10^{-16}

[30] B. Coqblin, J. Delaplace, V. Levy, A. A. Gomes, and J. Hillairet, J. Phys. (Paris) **28**, 75 (1967).
[31] J. Friedel, Trans. AIME **230**, 616 (1964).

TABLE IX. Comparison between spin-flip cross sections measured in this work and those obtained by other workers.

Alloy	This work	Other work
*Na*Hg	$(9.6\pm1.5)\times10^{-17}$	$(1.7\pm0.2)\times10^{-16}$ [a]
*Li*Mg	$(6.4\pm0.5)\times10^{-21}$	$(5.2\pm0.1)\times10^{-21}$ [b]
*Li*Zn	$(6.8\pm0.6)\times10^{-19}$	$(6.2\pm0.1)\times10^{-19}$ [b]
*Li*Ag	$(3.5\pm0.3)\times10^{-18}$	$(3.0\pm0.1)\times10^{-18}$ [b]
*Li*Ca	...	$\sim1.2\times10^{-21}$ [b]

[a] Garif'ianov and Starikov (Ref. 12).
[b] Hahn and Enderby (Ref. 12).

It is possible to rewrite Eq. (47) in a useful manner. For free atoms, the states $j=\frac{3}{2}$, $l=1$ and $j=\frac{1}{2}$, $l=1$ are split by the spin-orbit energy ΔE_{so}. Thus, since the phase shifts $\eta_j{}^l$ are functions of the energy of the electron, one can approximate the argument of the sine by

$$\eta_{3/2}{}^1-\eta_{1/2}{}^1=\Delta E_{\text{so}}(\partial\eta^1/\partial E)_{E_F}. \qquad (48)$$

Thus, we are in essence looking for a peak in the *derivative* of phase shift with energy.

Ferrell and Prange[32] (FP) have proposed the existence of a p-wave resonance (similar to those observed by Vassel and by Coqblin *et al.*) to explain the peak observed in $\sigma_{\text{spin-flip}}$. FP's explanation is semiquantitative, since it does not attempt to calculate the resonant behavior from first principles. It does give a very simple picture and provides a simple formula with only two adjustable parameters to describe all the data in one row of the periodic table for a given host. FP present a simple argument based on Friedel's sum rule and on the fact that the spin-flip cross section is proportional to the fourth power of the p component of the conduction wave function near the nucleus [see Eqs. (11) and (12)]. FP arrive at the following relation:

$$\sigma_{\text{spin-flip}}\alpha\sin^4\tfrac{1}{6}\pi(Z-Z_0), \qquad (49)$$

where

$$Z_0=2\eta_0/\pi+(10/\pi)\eta_2+1. \qquad (50)$$

Using Eq. (49), it is possible to obtain a remarkably good two-parameter fit to the data, as shown in Fig. 21. Using Eq. (47) together with the relation[33]

$$\tan\eta_{1\pm1/2}{}^1=\Gamma/2(E-E_\pm), \qquad (51)$$

which holds under the assumption that both p waves are in resonance, FP arrive at an estimate of the width Γ of the resonance,

$$\Gamma\approx3.6\pm0.6\text{ eV}.$$

If the scattering were *not* described by a simple resonance, the peak might correspond simply to a point of rapid change of the p-wave phase shifts [see Eq. (48)] *without* their having a large value.

[32] R. A. Ferrell and R. E. Prange, Phys. Rev. Letters **17**, 163 (1966).
[33] A. Messiah, *Quantum Mechanics* (John Wiley & Sons, Inc., New York, 1966), p. 398.

In the work of Vassel and of Coqblin *et al.*, the peak in the resistivity occurs near a valence configuration of s^2p^3 (arsenic). Odle and Flynn,[34] in work on the Knight shifts in liquid alloys of copper with copper-row solutes, have shown that the angular decomposition of the screening cloud (as deduced from the Friedel sum rule) for an impurity atom dissolved in a metal should be approximately the same as the screening in the free impurity atom (atomic screening hypothesis). In the metal, the quantity of screening by angular momentum l is given by

$$Z_l=(2/\pi)(2l+1)\eta_l. \quad (52)$$

This hypothesis is reasonable because the screening charge lies primarily within the atomic cell of the impurity atom. In this hypothesis, both η_0 and η_1 will be small for $Z=1$, and η_0 will increase steadily with Z until it reaches $\frac{1}{2}\pi$ and then remain fairly constant (see Paper II). Similarly, η_1 is small for small Z, but increases rapidly when η_0 becomes constant, passing through $\frac{1}{2}\pi$ when $Z=5$. Both here and in Paper II, models incorporating atomiclike screening give results that agree well with experiment for small Z. On the basis of this and other results,[34,35] we conclude that for impurities with small Z in monovalent metals the atomic screening hypothesis is substantially correct.

There are several difficulties with the FP resonance hypothesis. For example, when Au-row impurities are placed in Li (see Fig. 21):

$$Z_0\approx -1, \quad \eta_0+5\eta_2\approx -\pi, \quad \eta_1\approx\tfrac{1}{6}(Z+1)\pi. \quad (53)$$

But the fact that the η_0 and η_2 must remain constant as Z varies is in disagreement with the atomic screening hypothesis. Another difficulty occurs because FP's hypothesis requires $\eta_1\approx\frac{1}{2}\pi$ for valence differences as small as $+1$ (configuration s^2) or $+2$ (configuration s^2p). According to the atomic screening hypothesis, a p-wave phase shift of $\frac{1}{2}\pi$ implies screening by approximately 3 p electrons. Our calculations presented in Paper II confirm these views. If one accepts the FP description, the burden of understanding is then shifted to answering the question of where this extra p-type screening arises.

There appear to be two possible mechanisms that might give rise to p screening of the required magnitude. The first involves a repopulation effect in which the p-wave density is increased at the expense of the s wave and perhaps d wave. In this mechanism the core and s states float up to the Fermi surface, and thus one obtains a nonatomic configuration of screening for the core and s states. An example of this effect for Cu-row impurities in Al has recently been discussed by Rigney and Flynn.[35] From Knight-shift data, these authors estimate that 0.45 electron is missing from the d shell of Ga and Ge when dissolved in aluminum. Rigney and Flynn also interpret Knight-shift data for Hg, Tl, and Pb in liquid Na.[36] They find 2.5 to 3 p electrons necessary, whereas FP's hypothesis of a p-wave resonance requires 3.8 p electrons. The two numbers are reasonably close. However, as indicated above, the case of Pb in Li requires screening by 5 p electrons, which seems unlikely but not impossible, since Li and Pb come from different regions of the periodic table and have vastly different core structures.

The second mechanism leading to increased p-wave screening is the charging effect discussed theoretically by Stern.[37] He shows that the constituents of alloys in general have a different number of tight-binding approximation (TBA) electrons than the pure metals. The charging effect depends on the composition of the alloy and the ratio ϵ_{21}'/Δ, where ϵ_{21}' is the magnitude of the difference of the atomic energies of the two constituents of the alloy and Δ is the half-width of the band. For alkali-metal solvents and heavy normal-metal solutes, ϵ_{21}' can be quite large, so that we expect a large charging effect. Such charging means that the electronic density on neighboring sites is decreased, which is equivalent to making the phase shifts with $l\geq 2$ negative. Since the resulting electronic distribution due to the charging effect must conform to Friedel's sum rule, any charge transfer can only involve repopulation of the s, p, d, $\cdots$, partial waves. That such charge transfer occurs is manifested in the large number of ordered intermetallic compounds formed by lithium and sodium with heavy metals such as Hg and Pb. Experimental evidence for the charging effect in Au-Ag alloys (the Au becomes negatively charged) has become available from an NMR study by Narath.[38] He finds that the strength of the s-wave density at the Ag nucleus decreases by 30% from pure Ag to 5% Ag in Au.

It is possible that both of the two mechanisms discussed above are operative and can account for the anomalous nonmonotonic behavior of $\sigma_{\text{spin-flip}}$. In Paper II the possibility of a "size effect" is discussed and found to be of no importance. Further experimental data and calculations are needed before a complete understanding of the data is obtained.

ACKNOWLEDGMENTS

We would like to thank Dr. Joe Pifer for valuable suggestions about experimental technique, and E. Kevin Cornell for his help in the molten-state measurements.

APPENDIX: GENERAL OPW CALCULATION

Let us consider the five d-orbital states, which can be written

$$|q)=xy,\ xz,\ yz,\ x^2-y^2,\ 3z^2-r^2. \quad (A1)$$

For a plane wave traveling along the z axis, the only

[34] R. L. Odle and C. P. Flynn, Phil. Mag. **13**, 699 (1966).
[35] D. A. Rigney and C. P. Flynn, Phil. Mag. **15**, 1213 (1967).
[36] M. Hanabusa and N. Bloembergen, J. Phys. Chem. Solids **27**, 363 (1966).
[37] E. A. Stern, Physics **1**, 255 (1965).
[38] A. Narath, Phys. Rev. **163**, 232 (1967).

nonvanishing orthogonalization integral is

$$a_{nd}=(n,(3z^2-r^2)f(r)\,|e^{ikFz}). \tag{A2}$$

The average of the square of the matrix element is

$$\langle V_1^2\rangle_{F_{nd}}=\tfrac{1}{2}a_{nd}{}^4\sum_{q,q',q'',q'''}(q'|\lambda(r)l_x|q)$$
$$\times(q''|\lambda(r)l_x|q''')\int c_{q'Z'}{}^*c_{qZ}c_{q''Z}{}^*c_{q'''Z'}\frac{d\Omega d\Omega'}{(4\pi)^2}, \tag{A3}$$

where c_{qZ} is the coefficient relating the d function $|q)$ with the function $3Z^2-R^2$. We can write the rotated function as

$$R\psi_{lm}=\sum_{m'}D_{m'm}{}^l(\alpha,\beta,\gamma)\psi_{lm'}, \tag{A4}$$

where R is the rotation operator, and α, β, γ are the Euler angles. We can, without loss of generality, take $\gamma=0$, since we are concerned with the rotated functions ψ_{l0} (e.g., Z for a p state and $3Z^2-R^2$ for a d state). Let the axes X, Y, and Z (where $\mathbf{k}$ is taken along Z) make Euler angles α, β, 0 with x, y, and z. Thus

$$R\psi_{l0}=\sum_{m'}D_{m'0}{}^l(\alpha,\beta,0)\psi_{lm'}. \tag{A5}$$

Consider the quantity

$$(lm|\lambda(r)l_x|lm')(lm''|\lambda(r)l_x|lm''')$$
$$\times\int D_{m0}{}^{l*}(\alpha,\beta,0)D_{m'0}{}^l(\alpha',\beta',0)D_{m''0}{}^{l*}(\alpha',\beta',0)$$
$$\times D_{m'''0}{}^l(\alpha,\beta,0)\frac{d\Omega d\Omega'}{(4\pi)^2}. \tag{A6}$$

Now from Rose[39] we have

$$D_{m0}{}^l(\alpha,\beta,0)=[4\pi/(2l+1)]^{1/2}Y_{lm}{}^*(\beta,\alpha). \tag{A7}$$

Thus,

$$\int D_{m0}{}^{l*}(\alpha,\beta,0)D_{m'''0}{}^l(\alpha,\beta,0)\frac{d\Omega}{4\pi}$$
$$=\frac{1}{2l+1}\int Y_{lm}(\beta,\alpha)Y_{lm'''}{}^*(\beta,\alpha)d\Omega$$
$$=\frac{\delta_{m,m'''}}{2l+1}. \tag{A8}$$

[39] M. E. Rose, *Elementary Theory of Angular Momentum* (John Wiley & Sons, Inc., New York, 1957), p. 60.

The generalization of Eq. (A3) becomes

$$\langle V_1^2\rangle_{F_{nl}}=a_{nl}{}^4\tfrac{1}{2}\sum_{m,m'}|(lm|\lambda(r)l_x|lm')|^2/(2l+1)^2. \tag{A9}$$

If we quantize m along the $\bar{x}$ axis, all matrix elements vanish except for $m=m'$:

$$\sum_{m,m'}(lm|\lambda(r)l_x|lm')(lm'|\lambda(r)l_x|lm)$$
$$=\sum_m|(lm|\lambda(r)l_x|lm)|^2m^2=\lambda_{nl}{}^2\sum_m m^2. \tag{A10}$$

Since the expectation value of $\lambda(r)$ is independent of m,

$$|(lm|\lambda(r)|lm)|=|(ll|\lambda(r)|ll)|=\lambda_{nl}. \tag{A11}$$

λ_{nl} is the spin-orbit coupling constant of the nl orbital. Also,

$$\sum_m m^2=T_r(l_x{}^2)=\tfrac{1}{3}l(l+1)(2l+1). \tag{A12}$$

The final result is

$$\langle V_1^2\rangle_{F_{nl}}=\frac{l(l+1)}{6(2l+1)}a_{nl}{}^4\lambda_{nl}{}^2. \tag{A13}$$

For p states, $l=1$ and

$$\langle V_1^2\rangle_{F_{np}}=\tfrac{1}{9}a_{np}{}^4\lambda_{np}{}^2, \tag{A14}$$

which agrees with our previous result [Eq. (32)]. For d states, $l=2$ and

$$\langle V_1^2\rangle_{F_{nd}}=\tfrac{1}{5}a_{nd}{}^4\lambda_{nd}{}^2. \tag{A15}$$

In general, we have

$$\langle V_1^2\rangle_F=\sum_{n,l}\frac{l(l+1)}{6(2l+1)}a_{nl}{}^4\lambda_{nl}{}^2. \tag{A16}$$

The appropriate generalization of Eq. (A16) which takes into account the possibility of configuration interactions is

$$\langle V_1^2\rangle_F=\sum_{n,n',l}\frac{l(l+1)}{6(2l+1)}a_{n'l}{}^2a_{nl}{}^2\lambda_{nl,n'l}{}^2, \tag{A17}$$

where

$$\lambda_{nl,n'l}=|(nl|\lambda(r)|n'l)|. \tag{A18}$$